THE INFLUENCE OF THERMOELECTRIC EFFECTS ON THE MAXIMUM TEMPERATURE IN A RADIALLY CONSTRICTED GAS DISCHARGE BETWEEN ELECTRODES

By P. W. SEYMOUR*

[*Manuscript received January* 9, 1961]

Summary

In an earlier paper the author provided a method for estimating the maximum temperature in a steady-state, centrally constricted, highly ionized deuterium discharge between electrodes. The analysis applied to discharges not too long, so that bremsstrahlung loss could be neglected compared to the main heat loss by conduction to the electrodes, and thermoelectric effects were not included.

Here the analysis is generalized to include thermoelectric effects, and carried through for strictly longitudinal flow, for which at every point within the discharge the heat flux vector $\mathbf{q}$ and the current density vector $\mathbf{j}$ are parallel to the magnetic field $\mathbf{H}$.

Again a simple continuity argument shows that $\mathbf{q}+V\mathbf{j}=0$, where V is the electric potential, but now the equipotential surface on which $\mathbf{q}=V=0$ is displaced from midway between the electrodes nearly to the cathode. In the linear case the maximum temperature is displaced somewhat from the midway position towards the anode. A similar remark applies to the constricted discharge. The important influence of inclusion of thermoelectric effects is that the maximum temperature is increased by approximately 14% for about the same applied voltage producing a given current in a particular discharge geometry. The characteristic relating the maximum temperature and resistance ratio ε and the radial compression ratio ν obtained in the earlier paper is not changed by thermoelectric effects. Comparison of voltage and also temperature versus distance characteristics for linear and constricted discharges without and with thermoelectric effects is given by means of graphs.

I. INTRODUCTION

In an earlier paper (Seymour 1961), referred to hereafter as S, a method was given for estimating the maximum temperature in a steady non-equilibrium state, centrally constricted, substantially ionized deuterium discharge between electrodes. The free boundary surface of the plasma was assumed thermally insulated when isolated from the walls of the discharge tube, and cooling was therefore by heat conduction to the electrodes, compared to which the bremsstrahlung loss was shown to be negligible if the discharge was not too long. Neglect of thermoelectric and other effects led to symmetry of the distributions of temperature and voltage about a median plane normal to the longitudinal axis of the discharge, on which the plasma temperature was assumed constant at its maximum value T_m.

With ω_e the electron gyrofrequency and τ_e the electron collision time, the estimation of maximum temperature in discharges having straight and hyperbolic

* Research School of Physical Sciences, Australian National University, Canberra.

current streamlines was made via a vector analysis for $\omega_e\tau_e \ll 1$, and a tensor analysis for $\omega_e\tau_e \gg 1$. For flow having **q** and **j** parallel to the magnetic field **H** at every point within the discharge (strictly longitudinal flow), it was seen that the results obtained for $\omega_e\tau_e \ll 1$ applied for all $\omega_e\tau_e$.

In this paper we examine the same cases as above, under the same approximations, except that we include thermoelectric effects by generalizing the previous analysis, which destroys the symmetry of the temperature and voltage distributions about the median plane. Since strictly longitudinal flow is considered, it is convenient and sufficient to employ a vector method only.

Initial consideration of the problem suggested that for simplicity thermoelectric effects should be excluded in the first attempt at solution, and included later if possible.

This solution procedure proved satisfactory, and showed that it was not desirable to combine the separate results obtained, hence the presentation of results in separate papers.

II. Isotropic Forms of j and q (Seebeck and Peltier Effects only included)

When the magnetic field **H** is negligible or parallel to the electric field **E** and the temperature gradient ∇T, the general equations for **j** and **q** include only the Seebeck and Peltier effects respectively, as in (3.8) and (3.9) of S. For $\omega_e\tau_e \ll 1$ these equations reduce to the isotropic forms

$$\mathbf{j} = \sigma\mathbf{E} + \alpha\nabla T, \tag{2.1}$$

and

$$\mathbf{q} = -K\nabla T - \beta\mathbf{E}, \tag{2.2}$$

where σ and K are the scalars obtained in Section IV (a) of S, and we have replaced Marshall's (1957) φ and ξ by Spitzer and Härm's (1953) α and $-\beta$ respectively, and used Table 1 (constructed from pp. 67 and 69 of Marshall's report) to show that $\alpha^{\mathrm{I}} = \alpha^{\mathrm{II}} = \alpha$, $\alpha^{\mathrm{III}} \sim 0$; $\beta^{\mathrm{I}} = \beta^{\mathrm{II}} = \beta$, $\beta^{\mathrm{III}} \sim 0$, when $\omega_e\tau_e \ll 1$.

Table 1

Components of the Thermoelectric Tensors

Components of $[\alpha]$	Components of $[\beta]$
$\alpha^{\mathrm{I}} = 1\cdot554\dfrac{kn_e e\tau_e}{m_e}$	$\beta^{\mathrm{I}} = 6\cdot38\dfrac{kn_e e\tau_e T}{m_e}$
$\alpha^{\mathrm{II}} = -1\cdot5\dfrac{kn_e e\tau_e}{m_e}\,\dfrac{\omega_e^2\tau_e^2 - 0\cdot966}{\omega_e^4\tau_e^4 + 6\cdot282\omega_e^2\tau_e^2 + 0\cdot933}$	$\beta^{\mathrm{II}} = 2\dfrac{kn_e e\tau_e T}{m_e}\,\dfrac{0\cdot5\omega_e^2\tau_e^2 + 2\cdot98}{\omega_e^4\tau_e^4 + 6\cdot282\omega_e^2\tau_e^2 + 0\cdot933}$
$\alpha^{\mathrm{III}} = -4\cdot3\dfrac{kn_e e\tau_e}{m_e}\,\dfrac{\omega_e\tau_e}{\omega_e^4\tau_e^4 + 6\cdot282\omega_e^2\tau_e^2 + 0\cdot933}$	$\beta^{\mathrm{III}} = -2\dfrac{kn_e e\tau_e T}{m_e}\omega_e\tau_e\left[\dfrac{1\cdot25\omega_e^2\tau_e^2 + 7\cdot627}{\omega_e^4\tau_e^4 + 6\cdot282\omega_e^2\tau_e^2 + 0\cdot933}\right]$

Comparing α and β with their values in a Lorentz gas, we find from Spitzer and Härm that when the atomic number $Z=1$,

$$\alpha=3\left(\frac{2}{\pi}\right)^{3/2}\frac{k^{5/2}T^{3/2}}{m_e^{1/2}e^3\ln\lambda}\gamma_T, \tag{2.3}$$

and

$$\beta=8\left(\frac{2}{\pi}\right)^{3/2}\frac{k^{5/2}T^{5/2}}{m_e^{1/2}e^3\ln\lambda}\delta_E, \tag{2.4}$$

where the electron charge e has been taken in e.s.u. Here α and β for an actual gas have been expressed in terms of their values in a Lorentz gas by means of the transport coefficients γ_T and δ_E, given by Spitzer and Härm as $\gamma_T=0\cdot2727$, $\delta_E=0\cdot4652$. Spitzer and Härm's α and β agree closely with those of Marshall, who, however, does not specifically relate actual and Lorentz gas values.

Writing (2.3) as

$$\alpha=\alpha_0T^{3/2}/\ln\lambda, \tag{2.5}$$

and (2.4) as

$$\beta=\beta_0T^{5/2}/\ln\lambda, \tag{2.6}$$

we obtain by inserting numerical values

$$\alpha_0=9\cdot285\times10^{-9}\text{ A cm}^{-1}\text{ deg}^{-5/2}, \tag{2.7}$$

and

$$\beta_0=4\cdot223\times10^{-8}\text{ J V}^{-1}\text{ cm}^{-1}\text{ s}^{-1}\text{ deg}^{-5/2}. \tag{2.8}$$

To complete these equations we recall from S, Section V, that

$$\sigma=\sigma_0T^{3/2}/\ln\lambda, \tag{2.9}$$

and

$$K=K_0T^{5/2}/\ln\lambda, \tag{2.10}$$

where

$$\sigma_0=1\cdot53\times10^{-4}\ \Omega^{-1}\text{ cm}^{-1}\text{ deg}^{-3/2}, \tag{2.11}$$

and

$$K_0=4\cdot396\times10^{-12}\text{ J s}^{-1}\text{ cm}^{-1}\text{ deg}^{-7/2}. \tag{2.12}$$

III. Solution of the Plasma Energy Equation for Strictly Longitudinal Flow

Again, the analysis of a general, constricted discharge having geometric symmetry about a chosen plane is conveniently handled by introduction of an orthogonal curvilinear coordinate system, which can be specialized later to deal with linear discharges and those having hyperbolic streamlines. Before developing these solutions, however, the form of the differential equation for strictly longitudinal flow to be finally integrated can readily be obtained by a simple continuity argument.

(a) *Curved Stream Tube of a Constricted Discharge*

Figure 1 shows a curved current stream tube possessing geometric symmetry about a chosen plane. Suppose also that there exists an equipotential surface, normal to the curved axis of the tube, and nearer its lower end in Figure 1, on which $\mathbf{q}=0$ and on which it is convenient to take the constant electric potential as zero. Then, on that surface, with the notation of (5.15) of S, we have

$$\mathbf{M}=\mathbf{q}+V\mathbf{j}=0, \tag{3.1.1}$$

and since from (5.14) $\mathbf{M}$ is solenoidal, it follows that $\mathbf{M}$ vanishes identically at every point within the discharge, and the flow is longitudinal. Inserting (2.1) and (2.2) in (3.1.1), and using $\mathbf{E}=-\nabla V$, together with (2.5), (2.6), (2.9), and (2.10) above, we obtain

$$\nabla T/\nabla V=(\beta_0 T-\sigma_0 V)/(K_0 T-\alpha_0 V). \tag{3.1.2}$$

From the mode of derivation we see that this equation is valid for all values of $\omega_e\tau_e$ if $\mathbf{q}$ and $\mathbf{j}$ are at every point parallel to $\mathbf{H}$, i.e. if the flow is strictly longitudinal.

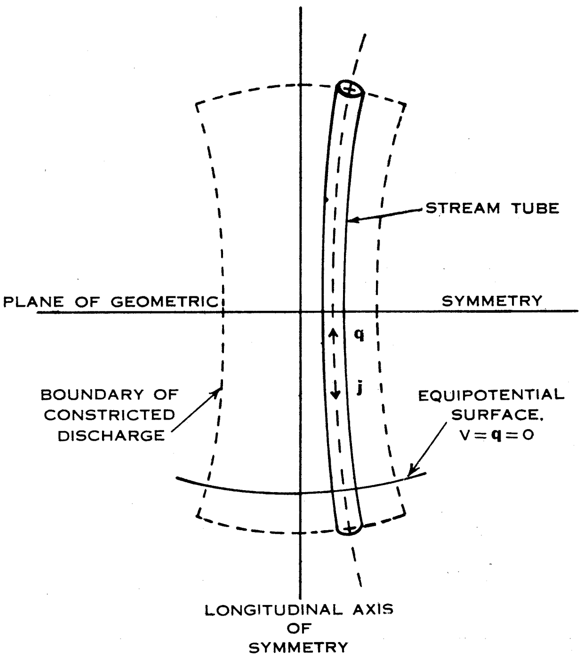

Fig. 1.—Curved stream tube of a constricted discharge.

(b) *Solution of a Simplified Form of the Plasma Energy Equation using Complex Variables*

For the detailed mathematical analyses of longitudinal flow the plasma energy equation, div $\mathbf{q}=\mathbf{j}\cdot\mathbf{E}$, is again simplified initially by introduction of the orthogonal curvilinear coordinates, ψ (the current stream function), φ, and V; and by consideration of axi-symmetric flow, as in S, Section VI (*b*). Integration leads to

$$\partial T/\partial V=(\beta_0 T-\sigma_0 V)/(K_0 T-\alpha_0 V), \tag{3.2.1}$$

which is a convenient form of (3.1.2).

A method of integrating (3.2.1) runs as follows : first introduce a parameter p, such that

$$\partial T/\partial p=\beta_0 T-\sigma_0 V, \tag{3.2.2}$$
$$\partial V/\partial p=K_0 T-\alpha_0 V. \tag{3.2.3}$$

Assume now that the physical temperature and electric potential are the imaginary parts of complex quantities $\overline{T}$ and $\overline{V}$ respectively, so that, if Im is the imaginary part operator,

$$T=\mathrm{Im}\ \overline{T}, \tag{3.2.4}$$

and

$$V=\mathrm{Im}\ \overline{V}. \tag{3.2.5}$$

Further, assume that

$$\overline{T}=A\mathrm{e}^{mp}, \tag{3.2.6}$$

and

$$\overline{V}=B\mathrm{e}^{mp}, \tag{3.2.7}$$

where m is a complex quantity.
Then

$$mA=\beta_0 A-\sigma_0 B, \tag{3.2.8}$$
$$mB=K_0 A-\alpha_0 B. \tag{3.2.9}$$

Combination of (3.2.8) and (3.2.9) yields

$$A/B=-\sigma_0/(m-\beta_0)=(m+\alpha_0)/K_0, \tag{3.2.10}$$

and hence, from the right-hand side equation,

$$m=\tfrac{1}{2}(\beta_0-\alpha_0)+\tfrac{1}{2}\mathrm{i}\{4K_0\sigma_0-(\alpha_0+\beta_0)^2\}^{\frac{1}{2}}, \tag{3.2.11}$$

where $4K_0\sigma_0-(\alpha_0+\beta_0)^2>0$, and the positive square root has been chosen for convenience of solution.

Writing

$$a=(\beta_0-\alpha_0)/\{4K_0\sigma_0-(\alpha_0+\beta_0)^2\}^{\frac{1}{2}}, \tag{3.2.12}$$

(3.2.11) becomes

$$m=\tfrac{1}{2}\{4K_0\sigma_0-(\alpha_0+\beta_0)^2\}^{\frac{1}{2}}(a+\mathrm{i}). \tag{3.2.13}$$

We now define a variable θ in terms of p as

$$\theta=\tfrac{1}{2}\{4K_0\sigma_0-(\alpha_0+\beta_0)^2\}^{\frac{1}{2}}p, \tag{3.2.14}$$

and then, on the permissible assumption that B is a real constant, write (3.2.7) as

$$V=B\mathrm{e}^{a\theta}\mathrm{e}^{\mathrm{i}\theta}, \tag{3.2.15}$$

and, with the aid of (3.2.10), write (3.2.6) as

$$T=\{(m+\alpha_0)/K_0\}B\mathrm{e}^{a\theta}\mathrm{e}^{\mathrm{i}\theta}. \tag{3.2.16}$$

Using (3.2.11), it is a simple proposition to show that

$$m+\alpha_0=(K_0\sigma_0)^{\frac{1}{2}}e^{i\varepsilon}, \tag{3.2.17}$$

where

$$\varepsilon=\tan^{-1}\left[\frac{\{4K_0\sigma_0-(\alpha_0+\beta_0)^2\}^{\frac{1}{2}}}{\alpha_0+\beta_0}\right]. \tag{3.2.18}$$

Hence, using (3.2.17), we may write (3.2.16) in the form

$$\overline{T}=(\sigma_0/K_0)^{\frac{1}{2}}\cdot Be^{a\theta}e^{i(\theta+\varepsilon)}. \tag{3.2.19}$$

Application of the operator Im to the equations (3.2.15) and (3.2.19) yields the physical electric potential and temperature expressions

$$V=Be^{a\theta}\sin\theta, \tag{3.2.20}$$

and

$$T=(\sigma_0/K_0)^{\frac{1}{2}}Be^{a\theta}\sin(\theta+\varepsilon). \tag{3.2.21}$$

To determine the real constant B, we observe that when $\partial T/\partial\theta=0$, $T=T_m$, the maximum temperature, and $\theta=\theta_m$. From (3.2.21), $\partial T/\partial\theta=0$ gives

$$\tan(\theta_m+\varepsilon)=-1/a. \tag{3.2.22}$$

Since ε and a can be calculated from the available data, θ_m is determined by (3.2.22). B is therefore obtained from (3.2.21) as

$$B=\frac{(K_0/\sigma_0)^{\frac{1}{2}}T_m}{(\exp a\theta_m)\sin(\theta_m+\varepsilon)}. \tag{3.2.23}$$

Proceeding numerically, use of equations (2.7), (2.8), (2.11), and (2.12) in (3.2.12) and (3.2.18) gives

$$\left.\begin{aligned} a&=5\cdot446,\\ \varepsilon&=0\cdot1169 \text{ radians } (6\cdot7^\circ). \end{aligned}\right\} \tag{3.2.24}$$

Insertion of these results into (3.2.22) gives

$$\theta_m=2\cdot8431 \text{ radians } (162\cdot9^\circ), \tag{3.2.25}$$

and so, using (2.11), (2.12), (3.2.24), and (3.2.25), (3.2.23) gives

$$B=1\cdot7713\times10^{-10}T_m \text{ deg}^{-1}\text{ V}, \tag{3.2.26}$$

and the factor $(\sigma_0/K_0)^{\frac{1}{2}}B$ becomes

$$(\sigma_0/K_0)^{\frac{1}{2}}B=1\cdot045\times10^{-6}T_m. \tag{3.2.27}$$

Substitution of these results in (3.2.20) and (3.2.21) yields the numerical forms

$$V=1\cdot7713\times10^{-10}T_m e^{5\cdot4460}\sin\theta \text{ V deg}^{-1}, \tag{3.2.28}$$

and

$$T=1\cdot045\times10^{-6}T_m e^{5\cdot4460}\sin(\theta+0\cdot1169). \tag{3.2.29}$$

If the thermoelectric coefficients α_0 and β_0 are excluded from (3.2.12) and (3.2.18),

$$\left.\begin{aligned} a&=0, \\ \varepsilon&=\tfrac{1}{2}\pi, \end{aligned}\right\} \tag{3.2.30}$$

and hence, from (3.2.22),

$$\theta_m=0. \tag{3.2.31}$$

With these results the expression (3.2.23) for B becomes simply,

$$B=(K_0/\sigma_0)^{\frac{1}{2}}T_m,$$

and accordingly (3.2.20) and (3.2.21) reduce respectively to

$$V=(K_0/\sigma_0)^{\frac{1}{2}}T_m \sin\theta, \tag{3.2.32}$$

and

$$T=T_m \cos\theta, \tag{3.2.33}$$

which can be combined to give

$$T^2+(\sigma_0/K_0)V^2=T_m^2, \tag{3.2.34}$$

as obtained in S, Section VI (*a*).

To complete the detailed mathematical analyses of non-constricted and constricted axi-symmetric discharges, we follow the procedure adopted in Section VI (*d*) of S, and introduce a more general orthogonal curvilinear coordinate system, w, v, u, and assume henceforth that V and T are functions of u only. Again, the only non-zero component of j is j_u, which, from (2.1), (2.5), (2.9), (3.2.14), (3.2.2), and (3.2.3), is given in curvilinear form as

$$j_u=\frac{2(\alpha_0\beta_0-K_0\sigma_0)}{\{4K_0\sigma_0-(\alpha_0+\beta_0)^2\}^{\frac{1}{2}}}\,\frac{T^{5/2}}{(h_3 \ln\lambda)}\,\frac{\partial\theta}{\partial u}, \tag{3.2.35}$$

or

$$j_u=G(u)/h_3, \tag{3.2.36}$$

where the notation adopted here is illustrated in Figure 2.

Integration of the steady-state form of the electrical equation of continuity, $\operatorname{div}\mathbf{j}=0$, gives, for axi-symmetric flow,

$$j_u=F(w)/h_1h_2. \tag{3.2.37}$$

Combination of (3.2.35) and (3.2.37) results in

$$F(w)\int_0^u \frac{h_3}{h_1h_2}\,du'=\frac{2(\alpha_0\beta_0-K_0\sigma_0)}{\{4K_0\sigma_0-(\alpha_0+\beta_0)^2\}^{\frac{1}{2}}}\,\frac{T_m^{5/2}}{\ln\lambda}\int_{\theta_1}^{\theta}\left(\frac{T}{T_m}\right)^{5/2}d\theta', \tag{3.2.38}$$

where we assume that the electrodes are held at $T=0$, so that from (3.2.21)

$$\left.\begin{aligned} &\theta_1 \text{ (at cathode)}=-0\cdot1169 \text{ radians } (-6\cdot7^\circ), \\ &\theta_2 \text{ (at anode)}\;\;\;=+3\cdot0246 \text{ radians } (+173\cdot3^\circ). \end{aligned}\right\} \tag{3.2.39}$$

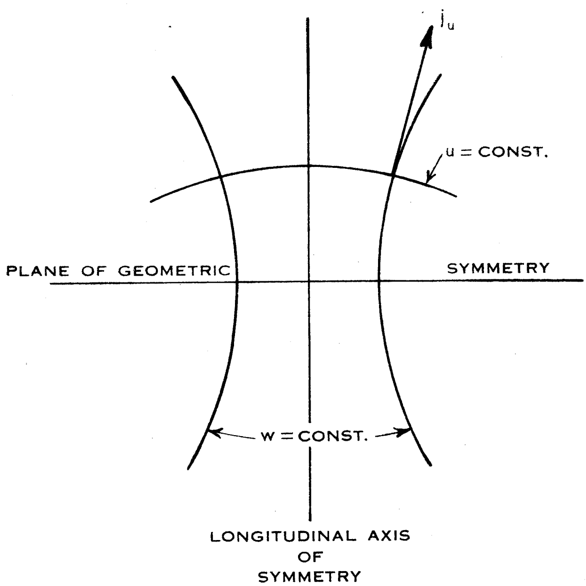

Fig. 2.—w and u as orthogonal curvilinear coordinates (axi-symmetric flow).

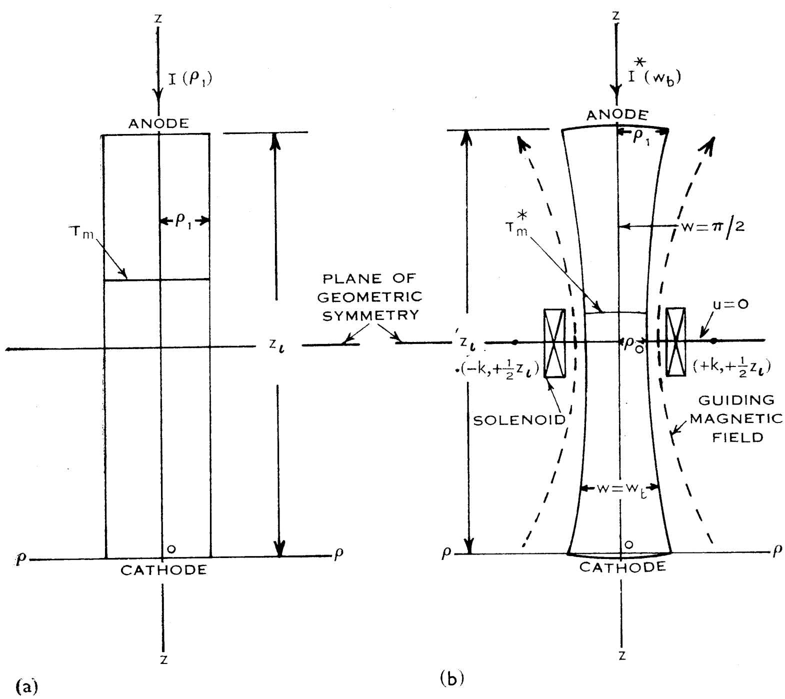

Fig. 3.—Discharge cross sections in the ρ-z plane. (a) Streamlines parallel to oz, (b) streamlines curved.

Equation (3.2.38) can be readily solved if the variables in $h_3/(h_1h_2)$ are separable. We now consider its application to (1) the linear, (2) the constricted discharge.

(c) *Specialization of Results for a Linear Discharge*

The cross section in the ρ-z plane for this case is shown in Figure 3 (*a*).

Using cylindrical coordinates, with $w=\rho$, $v=\varphi$, $u=z$, we have $h_1=h_3=1$, $h_2=\rho$, and $V=V(z)$, $T=T(z)$, $\psi=\psi(\rho)$. Thus, in Figure 3 (*a*) the streamlines are parallel to oz, and the equipotential lines are normal to oz. Using the above scale factors, (3.2.36) and (3.2.37) yield

$$j_z=G(z)=F(\rho)/\rho=\text{const.}, \tag{3.3.1}$$

and since (3.2.21) and (3.2.23) combine to give

$$\frac{T}{T_m}=\frac{(\exp a\theta)\sin(\theta+\varepsilon)}{(\exp a\theta_m)\sin(\theta_m+\varepsilon)},$$

use of the scale factors and these results in (3.2.38) gives

$$z=\frac{2(\alpha_0\beta_0-K_0\sigma_0)}{\{4K_0\sigma_0-(\alpha_0+\beta_0)^2\}^{\frac{1}{2}}}\frac{T_m^{5/2}}{j_z\ln\lambda}\int_{\theta_1}^{\theta}\left(\frac{(\exp a\theta')\sin(\theta'+\varepsilon)}{(\exp a\theta_m)\sin(\theta_m+\varepsilon)}\right)^{5/2}\mathrm{d}\theta', \tag{3.3.2}$$

or, using the earlier results for α_0, β_0, σ_0, K_0, and taking $\ln\lambda=10$,

$$z=-\frac{0\cdot9273}{10^8}\frac{T_m^{5/2}}{j_z}\int_{\theta_1}^{\theta}\left(\frac{(\exp a\theta')\sin(\theta'+\varepsilon)}{(\exp a\theta_m)\sin(\theta_m+\varepsilon)}\right)^{5/2}\mathrm{d}\theta'\ \mathrm{A\ cm^{-1}\ deg^{-5/2}}. \tag{3.3.3}$$

The value of the integral in the right-hand side of (3.3.3) can be obtained for chosen values of θ in the range $\theta_1<\theta\leqslant\theta_2$ by numerical integration, since a, ε, and θ_m are known. In particular, the length of the discharge, $z_\iota>0$, corresponds to $\theta=\theta_2$, and (3.3.3) then leads to

$$\frac{z}{z_\iota}=\frac{1}{0\cdot293}\int_{\theta_1}^{\theta}\left(\frac{(\exp a\theta')\sin(\theta'+\varepsilon)}{(\exp a\theta_m)\sin(\theta_m+\varepsilon)}\right)^{5/2}\mathrm{d}\theta'. \tag{3.3.4}$$

Equation (3.3.4) gives the fraction z/z_ι for each value of θ chosen, and therefore, using (3.2.28) and (3.2.29), V/T_m and T/T_m can be plotted against z/z_ι, as in Figure 4 (*b*). With reference to S, Section VI (*d*), we also include for comparison Figure 4 (*a*), which shows V/T_m and T/T_m plotted against z/z_0 when thermoelectric effects are excluded.

Examination of (3.2.35) for this case suggests the form $j_z=-j$, where $j>0$. Using this result, the maximum temperature is derived from (3.3.3) as

$$T_m=2228\{\tfrac{1}{2}z_\iota I(\rho_1)/\rho_1^2\}^{2/5}\quad\mathrm{A^{-2/5}\ cm^{2/5}\ deg}, \tag{3.3.5}$$

where $I(\rho_1)=\pi\rho_1^2j$, and the semi-length, $\frac{1}{2}z_\iota$, has been introduced to facilitate comparison of the above result with S, (6.4.14).

From (3.2.28) and (3.2.29), we have at the anode of the discharge,

$$V_2=+2\cdot434\times10^{-4}T_m\ \mathrm{V\ deg^{-1}}, \tag{3.3.6}$$

and at the cathode,

$$V_1=-1\cdot0933\times10^{-11}T_m\ \mathrm{V\ deg^{-1}}. \tag{3.3.7}$$

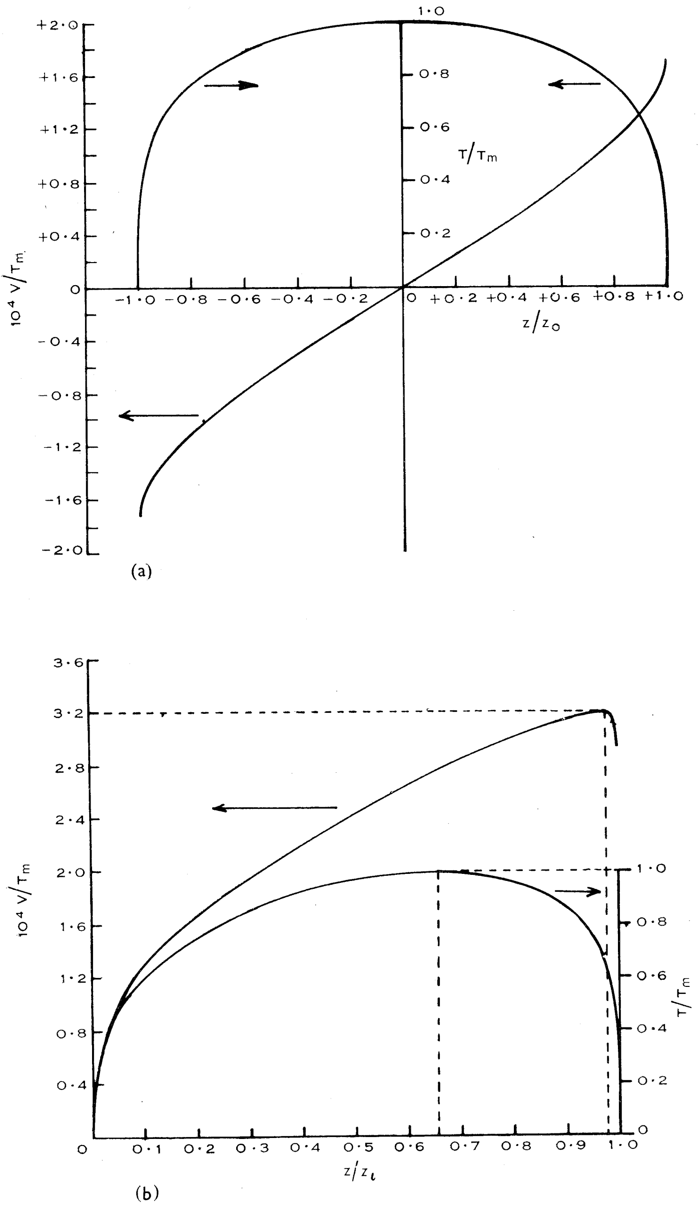

Fig. 4.—Temperature *v.* distance, voltage *v.* distance characteristics for linear discharge of circular cross section. (*a*) Thermoelectric effects excluded, (*b*) thermoelectric effects included.

The latter result shows that for values of T_m likely to be attained in practice, $V_1 \sim 0$, and accordingly the zero of potential may be conveniently considered located at the cathode. Then V_2 is the voltage across the discharge, and so, varying the subscript to ι,

$$T_m = 3397\, V_\iota\, \mathrm{V}^{-1}\ \mathrm{deg.} \tag{3.3.8}$$

Combination of (3.3.5) and (3.3.8) results in

$$V_\iota=0\cdot656\left(\frac{\frac{1}{2}z_\iota I(\rho_1)}{\rho_1^2}\right)^{2/5}\text{A}^{-2/5}\,\text{cm}^{2/5}\,\text{V}. \tag{3.3.9}$$

(*d*) *Specialization of Results for a Discharge having Hyperbolic Streamlines*

The cross section in the ρ-z plane for this case is shown in Figure 3 (*b*). The short solenoid producing the constricting, or guiding, magnetic field has axis oz, and is assumed centrally located between anode and cathode of the discharge. With $V=V(u)$, $\psi=\psi(w)$, we can again approximate the current streamlines by hyperbolae to represent the practical situation. Mathematically, we relate u and w to ρ and z by the conformal transformation

$$\rho+\mathrm{i}(z-\tfrac{1}{2}z_\iota)=k\cosh(u+\mathrm{i}w),\ k\text{ defined below,} \tag{3.4.1}$$

which expands to give

$$\rho=k\cosh u\cos w, \tag{3.4.2}$$

and

$$z-\tfrac{1}{2}z_\iota=k\sinh u\sin w. \tag{3.4.3}$$

Then

$$\rho^2/k^2\cosh^2 u+(z-\tfrac{1}{2}z_\iota)^2/k^2\sinh^2 u=1, \tag{3.4.4}$$

and

$$\rho^2/k^2\cos^2 w-(z-\tfrac{1}{2}z_\iota)^2/k^2\sin^2 w=1. \tag{3.4.5}$$

As in S, Section VI (*d*), Case 2, we see that in the ρ-z plane the curves $u=$const., $w=$const. form a family of confocal ellipses and hyperbolae, here with common foci at $(\pm k,\ +\frac{1}{2}z_\iota)$. Again, for the scale factors we have

$$h_1=h_3, \tag{3.4.6}$$

and

$$h_2=k\cosh u\cos w, \tag{3.4.7}$$

and accordingly, from (3.2.36), (3.2.37), and the above two equations

$$G(u)\cosh u=F(w)/k\cos w=\text{const.}=A. \tag{3.4.8}$$

Following the procedure of S, Section VI (*d*), we can establish

$$-I^*(w_b)=2\pi kA(1-\sin w_b). \tag{3.4.9}$$†

From Figure 3 (*b*) and equations (3.4.2), (3.4.3)

$$\left.\begin{aligned}\rho_0&=k\cos w_b,\\ \rho_1&=k\cosh u_e\cos w_b,\\ \tfrac{1}{2}z_\iota&=k\sinh u_e,\end{aligned}\right\} \tag{3.4.10}$$

where $u=\pm u_e$ gives the electrodes.

† The star superscript is used when necessary to indicate a Section III (*d*) quantity.

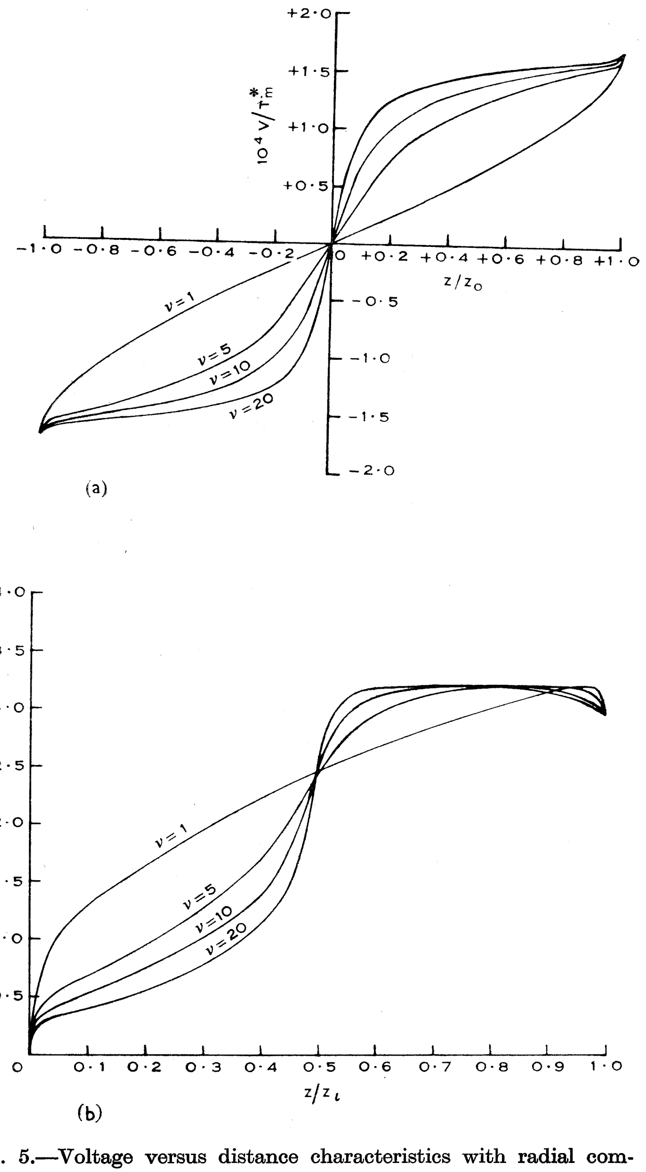

Fig. 5.—Voltage versus distance characteristics with radial compression ratio ν as parameter. (*a*) Thermoelectric effects excluded, (*b*) thermoelectric effects included.

By proper choice of the left-hand side integral limits in (3.2.38), and use of (3.2.21), (3.2.23), and (3.4.6) to (3.4.9), is obtained

$$\tan^{-1}(\sinh u)+\tan^{-1}(\sinh u_e)=$$

$$\frac{4\pi k(K_0\sigma_0-\alpha_0\beta_0)(1-\sin w_b)T_m^{*5/2}}{\ln \lambda I^*(w_b)\{4K_0\sigma_0-(\alpha_0+\beta_0)^2\}^{\frac{1}{2}}}\int_{\theta_1}^{\theta}\left(\frac{(\exp a\theta')\sin(\theta'+\varepsilon)}{(\exp a\theta_m)\sin(\theta_m+\varepsilon)}\right)^{5/2}\mathrm{d}\theta'. \tag{3.4.11}$$

With $u=+u_e$ corresponding to $\theta=\theta_2$, application to (3.4.11) of the steps that led to (3.3.4) yields

$$\frac{\tan^{-1}(\sinh u)+\tan^{-1}(\sinh u_e)}{2\tan^{-1}(\sinh u_e)}=\frac{1}{0\cdot 293}\int_{\theta_1}^{\theta}\left(\frac{(\exp a\theta')\sin(\theta'+\varepsilon)}{(\exp a\theta_m)\sin(\theta_m+\varepsilon)}\right)^{5/2}d\theta'=R \text{ say.} \tag{3.4.12}$$

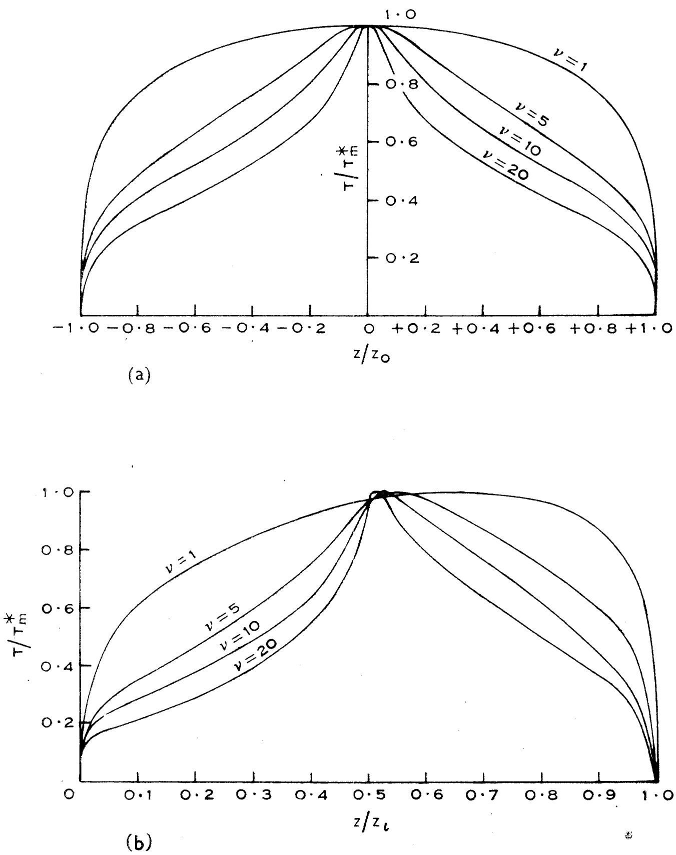

Fig. 6.—Temperature versus distance characteristics with radial compression ratio ν as parameter. (*a*) Thermoelectric effects excluded, (*b*) thermoelectric effects included.

When $w=\frac{1}{2}\pi$ we see from (3.4.2) and (3.4.3) that, as u varies, the point defined by the coordinates ρ and z moves along the symmetry axis oz in Figure 3 (*b*). Then, rearranging (3.4.12) and using (3.4.3) and the last equation of (3.4.10), we obtain

$$z/z_\iota=\tfrac{1}{2}[1+\{1/(\nu^2-1)^{\frac{1}{2}}\}\tan\{(2R-1)\tan^{-1}(\nu^2-1)^{\frac{1}{2}}\}], \tag{3.4.13}$$

where $\nu=\rho_1/\rho_0$ is the radial compression ratio. Clearly, $\nu=1$ reduces this equation to (3.3.4) as required.

Using appropriate numerical techniques we can obtain from (3.4.13) the fraction z/z_ι for each value of θ chosen, with ν as a parameter, and hence, with the further aid of (3.2.28) and (3.2.29), V/T_m^* and T/T_m^* can be plotted versus z/z_ι for suitable values of ν, as in Figures 5 (*b*) and 6 (*b*) respectively. Similarly, with reference to S, (6.4.33), and the associated expressions $T=T_m^* \cos\theta$, $V=(K_0/\sigma_0)^{\frac{1}{2}}T_m^* \sin\theta$, $-\frac{1}{2}\pi \leqslant \theta \leqslant +\frac{1}{2}\pi$, we can calculate for comparison the characteristics of Figures 5 (*a*) and 6 (*a*), which show respectively V/T_m^* and T/T_m^* versus z/z_0 when thermoelectric effects are excluded.

Using the corresponding values $u=+u_e$ and $\theta=\theta_2$, the maximum temperature is derived from (3.4.11) as

$$T_m^* = \left(\frac{\ln \lambda I^*(w_b)\{4K_0\sigma_0-(\alpha_0+\beta_0)^2\}^{\frac{1}{2}} \tan^{-1}(\sinh u_e)}{(0\cdot 293)2\pi k(1-\sin w_b)(K_0\sigma_0-\alpha_0\beta_0)}\right)^{2/5}. \tag{3.4.14}$$

The results (3.4.10) can be interpreted geometrically with the aid of Figure 3 (*b*) as in S, Section VI (*d*), and (3.4.14) accordingly becomes

$$T_m^* = \left(\frac{\ln \lambda I^*(w_b)\{4K_0\sigma_0-(\alpha_0+\beta_0)^2\}^{\frac{1}{2}}(\nu^2-1)^{\frac{1}{2}} \tan^{-1}(\nu^2-1)^{\frac{1}{2}}}{(0\cdot 293)2\pi(\frac{1}{2}z_\iota)(K_0\sigma_0-\alpha_0\beta_0)[1-\{1-(\rho_1/\frac{1}{2}z_\iota)^2\nu^{-2}(\nu^2-1)\}^{\frac{1}{2}}]}\right)^{2/5}. \tag{3.4.15}$$

Again referring to (2.7), (2.8), (2.11), (2.12); taking $\ln\lambda=10$, and from physical considerations, $(\rho_1/\frac{1}{2}z_\iota)^2 \ll 1$, (3.4.15) reduces to the more attractive form

$$T_m^* = 2228\left\{\frac{\frac{1}{2}z_\iota I^*(w_b)}{\rho_1^2}\right\}^{2/5}\left\{\frac{\nu^2 \tan^{-1}(\nu^2-1)^{\frac{1}{2}}}{(\nu^2-1)^{\frac{1}{2}}}\right\}^{2/5} \mathrm{A}^{-2/5}\,\mathrm{cm}^{2/5}\,\mathrm{deg}. \tag{3.4.16}$$

Combining (3.4.16) with (3.3.8), which is also applicable here,

$$V_\iota^* = 0\cdot 656\left\{\frac{\frac{1}{2}z_\iota I^*(w_b)}{\rho_1^2}\right\}^{2/5}\left\{\frac{\nu^2 \tan^{-1}(\nu^2-1)^{\frac{1}{2}}}{(\nu^2-1)^{\frac{1}{2}}}\right\}^{2/5} \mathrm{A}^{-2/5}\,\mathrm{cm}^{2/5}\,\mathrm{V}. \tag{3.4.17}$$

IV. Discussion of Results

To estimate the influence of thermoelectric effects, we first take from S the results (6.4.38) and (6.4.40), and combine them with (3.4.16) and (3.4.17) above to obtain for a given discharge the ratios

$$\tilde{T}_m^*/T_m^* = 1\cdot 136, \qquad (4.1)\dagger$$

and

$$\tilde{V}_\iota^*/2V_e^* = 0\cdot 985. \tag{4.2}$$

Comparing Figures 4 (*a*) and 4 (*b*), we observe that, for the linear discharge, inclusion of thermoelectric effects results in a displacement of the zero of the heat flux vector and electric potential from midway between the electrodes virtually to the cathode. Also, in Figure 4 (*b*) it is evident that the slope of the electric

† The curly bar is used when necessary to indicate a thermoelectric case quantity.

potential characteristic changes sign near the anode, and so, from (2.1), we see that in this region the constant current density **j** of the linear discharge is maintained by the term $\alpha\nabla T$ acting against $\sigma\mathbf{E}$. By forming the scalar product $\mathbf{j}\cdot\mathbf{E}$, we see that the Joule heating per unit volume in this region is made up of a cooling term, $\alpha\mathbf{E}\cdot\nabla T$, and a smaller heating term, σE^2. Considering the nature of the Seebeck and Peltier effects included in the basic equations (2.1) and (2.2) for **j** and **q**, this is perhaps not a surprising result.

Since, for the linear discharge, $q_z+Vj_z=0$, where the current density $j_z=-j$, $j>0$, is a constant, it is of interest to note that the voltage characteristics of Figures 4 (*a*) and 4 (*b*) also represent the heat flux characteristics $q_z/(jT_m)$ plotted against z/z_0 and z/z_ι respectively.

Further comparison of Figures 4 (*a*) and 4 (*b*) shows that thermoelectric effects displace the temperature maximum from midway between the electrodes towards the anode, but here the displacement is not marked.

When the discharge is constricted at the plane of geometric symmetry and thermoelectric effects are excluded, the shape of the temperature versus distance characteristic varies with increase of radial compression ratio, as shown in Figure 6 (*a*). Since the central constriction produces an increase of plasma temperature at and near the plane of symmetry, the narrowing of the peaks of the characteristics in Figure 6 (*a*) with increase of radial compression ratio can be readily understood physically.

Figure 6 (*b*) gives corresponding characteristics when thermoelectric effects are included. Broadly, the above remark on Figure 6 (*a*) applies here, and, as would also be expected from physical reasoning, the displaced temperature maximum of the linear discharge tends to return towards the plane of geometric symmetry as the radial compression ratio assumes values greater than unity.

As can be verified by means of (3.2.36), (3.4.8), and S, (6.4.22), when the discharge is centrally constricted the current density is no longer constant, but becomes a function of w and u. This remark also applies when thermoelectric effects are excluded, as can be seen from S, (6.4.5), (6.4.22), and (6.4.26). These and other facts complicate the possibility of obtaining a simple physical explanation of the trend of the voltage against distance characteristics of Figures 5 (*a*) and 5 (*b*) as radial compression increases.

The important conclusion that can be drawn from equation (4.1) is that the maximum temperature $\tilde{T}_m^*$ is raised above T_m^* by some 14% due to thermoelectric effects. However, by forming the temperature ratio, $\tilde{T}_m^*/\tilde{T}_m$, from (3.4.16) and (3.3.5); and the resistance ratio, $\tilde{R}^*/\tilde{R}$, from (3.4.17) and (3.3.9) for conditions outlined in S, Section VII, it is immediately evident that the characteristic of Figure 7 of that paper is also applicable when thermoelectric effects are included.

Equation (4.2) shows that the total voltage required to produce a given current in a particular geometry of discharge is about the same without and with thermoelectric effects.

V. Acknowledgment

Progress in the attempt to include thermoelectric effects in the analysis of the steady-state deuterium discharge cooled by heat flow to the electrodes was aided by discussions with Professor K. J. Le Couteur, and the author gratefully acknowledges the guidance and helpful suggestions received at these discussions.

VI. References

Marshall, W. (1957).—Kinetic theory of an ionized gas. Part 3, p. 91. Atomic Energy Research Establishment Report T/R 2419. (H.M. Stationery Office : London.)

Seymour, P. W. (1961).—Estimation of the maximum temperature in a radially constricted gas discharge between electrodes. *Aust. J. Phys.* **14** : 129–51.

Spitzer, L., Jr., and Härm, R. (1953).—Transport phenomena in a completely ionized gas. *Phys. Rev.* **89** : 977–81.